

Spectral analysis of mixing in 2D high-Reynolds flows

Hassan Arbabi¹†, Igor Mezić²

¹Department of Mechanical Engineering, Massachusetts Institute of Technology
Cambridge, MA 02139, USA

²Department of Mechanical Engineering, University of California Santa Barbara
Santa Barbara, CA 93106, USA

We use spectral analysis of Eulerian and Lagrangian dynamics to study the advective mixing in an incompressible 2D bounded cavity flow. A significant property of this flow at high Reynolds numbers is that mixing in its rotational core is slower than wall-adjacent areas and corner eddies. We explain this property by appealing to the Prandtl-Batchelor theorem for unsteady flows which predicts a flat distribution of tracer circulation periods in the core of mean flow — similar to rigid body rotation — at high Reynolds numbers. When this inviscid core is exposed to velocity fluctuations arising from bifurcation at high Reynolds, it shows more resilience toward resonance in Lagrangian motion and hence mixes more slowly compared to other areas.

We also investigate how well the truncations of Koopman mode decomposition and proper orthogonal decomposition approximate the mixing process in the flow. For periodic and quasi-periodic flows, the mixing is accurately explained by models comprising of a few Koopman modes, while for flows with aperiodic time dependence, the number of modes required to represent the mixing is substantially larger.

1. Introduction

Mixing is an important aspect of many natural and industrial flows. Characterizing the vertical mixing in the ocean and atmosphere, for example, constitutes the main challenge in modeling the earth climate ([Large *et al.* 1994](#); [Sherwood *et al.* 2014](#)), while understanding the horizontal mixing on the ocean surface helps us predict the movement of pollution and could lead to more effective strategies for containment ([Coulliette *et al.* 2007](#)). Other examples from natural flows include the mixing in the earth mantle which led to formation of oceanic islands with nonuniform geochemistry ([Ferrachat & Ricard 2001](#)), blood flow mixing in relation to health and disease ([Shadden & Taylor 2008](#)) and the role of mixing in shaping the ecological equilibrium in oceanic environment ([Valentine *et al.* 2012](#)). For the industrial flows, on the other hand, we often try to manipulate mixing, e.g., design devices that efficiently mix the fluids given the constraints by the specific application ([Khakhar *et al.* 1987](#); [Stroock *et al.* 2002](#)). All such efforts are based on our understanding of many factors that play a role in mixing like the flow dynamics, device geometry and initial configuration of the mixing fluids.

Study of mixing in real-world problems is difficult. Most of rigorous analysis in this field comes from the theory of chaotic advection, which treats the motion of tracers in the flow as a dynamical system ([Aref 1984](#); [Ottino 1989](#); [Rom-Kedar *et al.* 1990](#)). This theory

† Email address for correspondence: arbabi@mit.edu, mezić@ucsb.edu

has had a great influence on how we view the transport of material in flows which are steady or time-periodic, but it offers significantly less insight for flows which are *aperiodic* in time. On the other hand, most of the natural flows and many industrial flows show aperiodic time dependence. As a result, a large number of techniques have been devised to fill the gap between the knowledge of mixing in periodic flows and the aperiodic flows that appear in practice. Most of these techniques strive to characterize the mixing in a given aperiodic flow by detecting the coherent structures and visualizing the flow in a way that is most informative about the collective behavior of Lagrangian trajectories. Those techniques, just to name a few, include the theory of Lagrangian coherent structures (Haller 2015), topological analysis via braid dynamics (Boyland *et al.* 2000; Budišić & Thiffeault 2015), theory of finite-time coherent sets (Froyland *et al.* 2010), and ergodic theoretic analysis by time averaging (Poje *et al.* 1999).

In this work, we study the connection between the flow dynamics, i.e., the time evolution of the velocity field, and advective mixing of passive tracers in a 2D flow. In particular, we apply our analysis to lid-driven flow in a square cavity obtained from numerical simulation. This flow bifurcates into periodic, quasi-periodic and ultimately chaotic dynamics with the increase of Reynolds numbers. An important feature of these time-dependent flows is that at very high Reynolds numbers the vorticity approaches a uniform distribution in their rotating core. This is known as Prandtl-Batchelor theorem (Prandtl 1904; Batchelor 1956) and was recently extended to unsteady flows by Arbabi & Mezić (2019). In this paper, we show that this uniform distribution of vorticity leads to uniform distribution of Lagrangian time periods in the mean flow, and that leads to weaker mixing in the core, compared to areas adjacent to the walls and secondary vortices. This behavior is in stark contrast to mixing at low Reynolds where mixing is stronger away from the walls, and we expect it to hold true for other 2D high-Reynolds flows with rotational structure.

We also investigate how the complexity of mixing process is changed while the temporal regime of the lid-driven cavity flow changes from steady to aperiodic. We use a combination of Koopman Mode Decomposition (KMD) and Proper Orthogonal Decomposition (POD) to extract the hierarchy of the energetic modes in the flow, and use subsets of those modes to build finite-dimensional projection models to approximate the flow evolution. Then we quantify how mixing in those models mimic the mixing in the actual flow. This will reveal the effect of different modes on mixing, and characterize the dimensionality of models required to replicate mixing in complex flows.

The procession of ideas in this paper are as follows: we first give an account of the previous studies on mixing in lid-driven cavity flow. In section 2, we specify the geometry and dynamics of the lid-driven cavity flow in our study. We also present the spectral analysis of the flow field for each temporal regime that appears due to the flow bifurcations with the increase of Reynolds number. In section 3, we introduce our tools for mixing analysis: section 3.1 reviews the application and computation of hypergraphs for visualization of mixing in a given flow. Section 3.2 discusses quantitative analysis of mixing using the mix-norm. We present the qualitative picture of mixing in cavity flow in section 4 and discuss the role of Prandtl-Batchelor theorem leading to weak mixing in the core. In section 5, we describe our experiment for analysis of modal contributions to mixing and present its results.

1.1. Previous studies on mixing in lid-driven cavity flow

The mixing in the lid-driven cavity flow has been explored from many aspects and under different settings. This flow requires a simple computational setup and it is regularly used as a computational benchmark problem (Ghia *et al.* 1982). It is also studied

via experiments in 2D (Gharib & Derango 1989) and 3D geometry (Koseff & Street 1984). The 2D flow which we focus on here represents a simplified model of geophysical flows driven by surface shear (Tseng & Ferziger 2001), or common types of mixers in polymer engineering (Chella & Ottino 1985). Most of the previous studies have focused on low-Reynolds cavity flows with time-dependent lid motion, and investigated the effect of different factors like lid motion frequency and cavity geometry on enhancement of mixing.

In the steady lid-driven cavity flow, which is the stable solution at low Reynolds, mixing is generally poor since the tracers are confined to move along the streamlines (Ottino 1989). The experiments by Chien *et al.* (1986) and Leong & Ottino (1989) showed that mixing is greatly improved if periodic lid motion is used to generate periodic flow. In that case, the motion of tracers inside the cavity is comprised of both periodic and chaotic trajectories. The chaotic trajectories make the well-mixed regions while the tracers with periodic motion form coherent patches of fluid called *periodic islands*. These islands prevent full mixing because the fluid blobs remain trapped inside them and do not spread over the cavity. The experiments showed that size of these islands are dependent on the forcing frequency, and it was understood that there are optimal frequencies, at which, the islands would vanish and complete mixing could be achieved. Ling & Schmidt (1992) and Ling (1993) identified such frequency ranges by studying the linear stability of the periodic orbits corresponding to those islands. Their results showed good agreement with simulation and previous experiments, and motivated further studies on detection of periodic orbits in the cavity and their role in mixing (see e.g. Jana *et al.* 1994a; Meleshko & Peters 1996; Anderson *et al.* 1999, 2000; Stremmer & Chen 2007).

The aperiodic mixing is much less explored in the studies regarding the lid-driven cavity flow. Franjone *et al.* (1989) and Ottino *et al.* (1992) proposed a non-random aperiodic protocol for the lid motion to enhance mixing. The underlying idea in their work is to manipulate the symmetries in the flow to break up the periodic islands. The numerical studies by Liu *et al.* (1994) also showed that the aperiodic lid motion can lead to stronger and more uniform mixing in the cavity flow. We note that the aperiodicity of the flow in the above studies is generated by modulating the lid velocity, whereas in our study, the aperiodicity arises due to Navier-Stokes dynamics at high Reynolds number while the lid velocity is constant.

There are also a number of studies that investigated the mixing in lid-driven cavity flow, with different geometries (Ottino *et al.* 1992; Jana *et al.* 1994b; Migeon *et al.* 2000), or under the effect of flow stratification (Tseng & Ferziger 2001), multi-phase flow configuration (Chakravarthy & Ottino 1996; Chella & Viñals 1996), and motion of freely moving solid bodies within the flow (Vikhansky 2003; Hwang *et al.* 2005; Pai *et al.* 2013).

2. Dynamics of lid-driven cavity flow

We use a data-driven approach based on the spectral analysis of Koopman operator to characterize and present the cavity flow dynamics. The idea of Koopman operator goes back to Koopman (1931), while its application for data-driven analysis of high-dimensional systems was proposed just in the last decade (Mezić & Banaszuk 2004; Mezić 2005). In particular, Mezić (2005) introduced the notion of Koopman modes, which are analogues of eigenvectors in linear systems, for nonlinear evolution of spatio-temporal systems like fluids. Rowley *et al.* (2009) pioneered the data-driven Koopman approach for fluid flows and pointed out the connection between Koopman mode decomposition (KMD) and the dynamic mode decomposition algorithm (Schmid 2010). In a previous work, we used KMD to categorize and study different dynamic regimes of the cavity flow

(Arbabi & Mezić 2017). The key to understanding the flow regime (i.e the geometry of attractor in the state space of the flow) is the Koopman spectrum, while the Koopman modes reveal the associated spatial structures in the flow domain. Here we review those results and recount the sequence of flow regimes that appear with the increase of Reynolds number in the cavity flow.

The cavity flow domain is a square box $[-1, 1]^2$ with fixed walls except at the top where the wall moves with the velocity profile

$$u_{top}(x) = (1 - x^2)^2, \quad -1 \leq x \leq 1. \quad (2.1)$$

We define the Reynolds number as

$$Re = \frac{L_c U_c}{\nu} = \frac{2}{\nu}, \quad (2.2)$$

where $L_c = 2$ and $U_c = 1$ are the characteristic length and velocity respectively, and ν denotes the fluid kinematic viscosity in the numerical simulation.

Figure 1 summarizes the dynamics of cavity flow as explained by the Koopman spectrum of flow field data. For low Reynolds numbers, the flow started from zero initial condition converges to a steady solution. At a Reynolds number slightly above 10000, a Hopf bifurcation occurs and the asymptotic flow dynamics becomes periodic, i.e., the trajectory in the state space of the flow converges to a limit cycle. The Koopman frequencies for the periodic flow consist of a basic frequency ω_1 (frequency of limit cycle in the state space) and its multiples $\omega_k := k\omega_1$ with $k \in \mathbb{Z}$. The evolution of velocity field with time is described by the KMD of the form

$$\mathbf{u}^p(x, y, t) = \mathbf{u}_0(x, y) + \sum_{\substack{k \in \mathbb{Z} \\ k \neq 0}} \mathbf{u}_k^p(x, y) e^{ik\omega_1 t}, \quad (2.3)$$

where \mathbf{u}_k is the Koopman mode of velocity field associated with Koopman frequency $k\omega_1$ and \mathbf{u}_0 is the mean flow (i.e. the Koopman mode associated with zero frequency). Three Koopman modes of the periodic flow with highest kinetic energy are depicted in the first row of fig. 2.

At a Reynolds number slightly above 15000, the flow undergoes another Hopf bifurcation and becomes quasi-periodic. The quasi-periodic flow exhibits two basic frequencies $\boldsymbol{\omega} = (\omega_1, \omega_2)$, and the Koopman frequencies are the linear combination of the basic frequencies with integer coefficients $\mathbf{k} = (k_1, k_2)$, i.e., $\omega_{\mathbf{k}} := k_1\omega_1 + k_2\omega_2$ with $k_1, k_2 \in \mathbb{Z}$. The KMD for the quasi-periodic velocity field is given by

$$\mathbf{u}^q(x, y, t) = \mathbf{u}_0(x, y) + \sum_{\substack{\mathbf{k} \in \mathbb{Z}^2 \\ \mathbf{k} \neq (0,0)}} \mathbf{u}_{\mathbf{k}}(x, y) e^{\mathbf{k} \cdot \boldsymbol{\omega} t}, \quad (2.4)$$

with the notation similar to (2.3). Figure 2 shows the mean flow and the basic oscillatory Koopman modes (i.e modes associated with the two basic frequencies).

As the Reynolds number is increased higher than 18000, the Koopman spectrum becomes mixed, that is, a combination of discrete frequencies that describe the quasi-periodicity and the continuous spectrum which corresponds to the chaotic components of the velocity field. The Koopman mode decomposition for this flow reads

$$\mathbf{u}^m(x, y, t) = \mathbf{u}_0(x, y) + \sum_{\substack{\mathbf{k} \in \mathbb{Z}^2 \\ \mathbf{k} \neq (0,0)}} \mathbf{u}_{\mathbf{k}}(x, y) e^{\mathbf{k} \cdot \boldsymbol{\omega} t} + \mathbf{u}_c(x, y, t), \quad (2.5)$$

with \mathbf{u}_c denoting the chaotic component of the velocity field. Note that for this flow it is

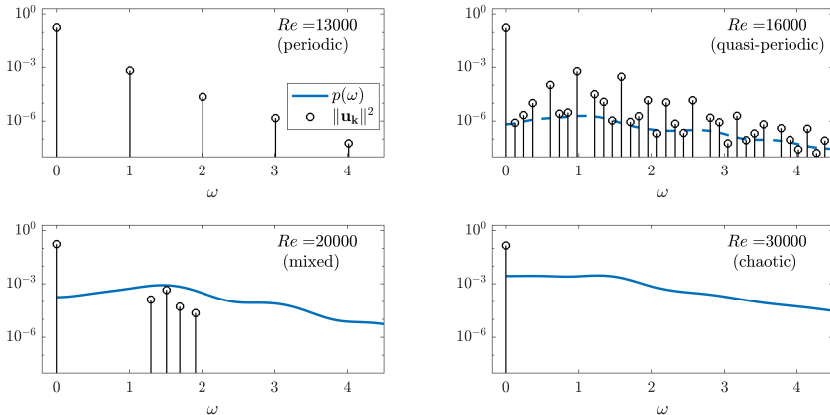


FIGURE 1. Flow dynamics revealed by Koopman spectrum of data: In periodic and quasi-periodic flow the Koopman frequencies (circles) are multiples of the one or two basic frequencies (top panels), in chaotic flow the only Koopman discrete frequency is zero and the rest of energy is in the continuous spectrum (bottom right), and for cavity flow there exists an intermediate range with mixed spectra (bottom left).

difficult to detect the true modes within background chaos and fig. 1 shows the modes that have passed the robustness test described in Arbabi & Mezić (2017). In the same figure, the strength of the continuous spectrum and chaotic component is reflected by the Koopman spectral density $p(\omega)$ which is similar to power spectral density of stationary processes. For more on continuous spectrum expansion see Mezić (2013).

As the Reynolds number is increased even further, the continuous spectrum becomes more dominant so that no quasi-periodic components can be found for Reynolds numbers above 22000. Then the KMD consists only of the mean flow and the chaotic component, i.e.,

$$\mathbf{u}^a(x, y, t) = \mathbf{u}_0(x, y) + \mathbf{u}_c(x, y, t). \quad (2.6)$$

There are two observations of Koopman modes of the flow which are important for study of mixing. First, vorticity in the core of mean flow is constant and it is zero in the core of oscillatory modes (fig. 2 and 3). This is a consequence of Prandtl-Batchelor theory and we will discuss it in the results. Second observation is that linear relationships between different observable fields carries over to the Koopman modes of those observables. For example, the stream function ψ and velocity field \mathbf{u} are related via the linear operator $\nabla^\perp := [\partial/\partial y, -\partial/\partial x]^T$ such that $\mathbf{u} = \nabla^\perp \psi$. Now if we let ψ_j and \mathbf{u}_j denote the Koopman modes of these two observable fields associated with Koopman frequency ω_j , then

$$\mathbf{u}_j = \nabla^\perp \psi_j. \quad (2.7)$$

This also implies that the KMD of those observables contain the same Koopman frequencies (as long as no ψ -mode is in the null space of ∇^\perp), and the Koopman modes describe the same steady flow field. Therefore, when we study the effect of the Koopman mode associated with frequency ω_j on mixing, we can switch between different representations of that mode including the stream function mode, velocity mode and also vorticity mode. Note that in this work, we identify complex conjugate pairs of Koopman modes with their common frequency.

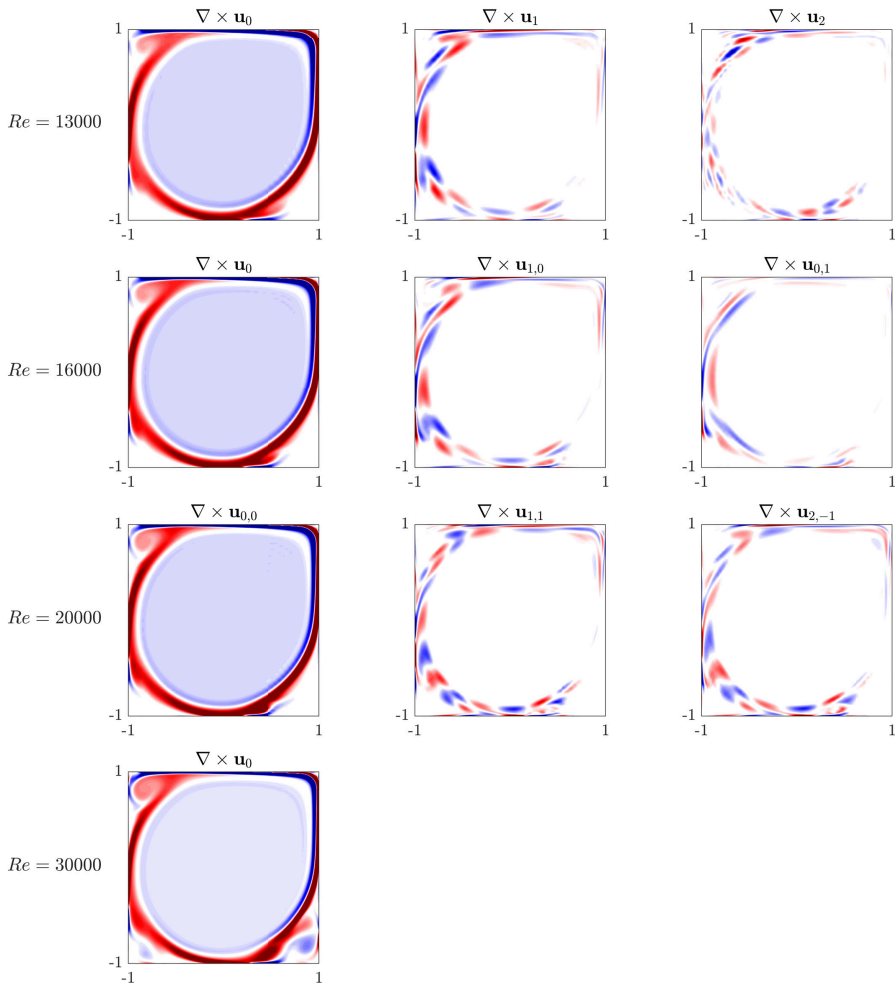


FIGURE 2. The (real part of) Koopman modes of vorticity for cavity flow. Clockwise rotation is marked with blue and counterclockwise with red.

2.1. POD of chaotic components

The chaotic part of the velocity field which is present in the high-Reynolds flows, does not admit a decomposition into Koopman modes. However, the chaotic component of a post-transient flow (i.e. evolving on the attractor) is a realization of a stationary stochastic process and therefore we can use statistical tools such as POD to obtain a meaningful decomposition. POD is a linear decomposition of the flow field into spatially orthogonal modes and uncorrelated temporal coefficients (Holmes *et al.* 2012). The POD for the chaotic component $\mathbf{u}_c(x, y, t)$ is denoted by

$$\mathbf{u}_c(x, y, t) = \sum_k a_k(t) \phi_k(x, y), \quad (2.8)$$

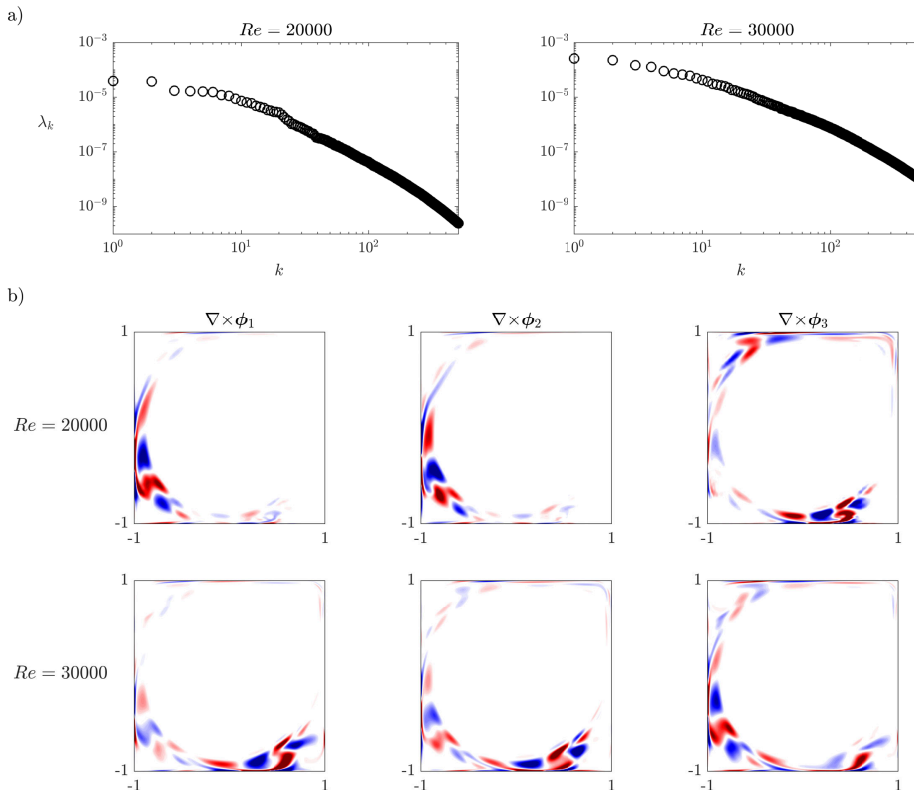


FIGURE 3. POD of the chaotic component: a) POD eigenvalues (i.e. kinetic energy of normalized POD modes), b) the vorticity field of 3 most energetic POD modes. The number of POD modes (in addition to Koopman modes of quasi-periodic part) required to resolve %99 of unsteady kinetic energy is 43 and 186 for $Re = 20000$ and $Re = 30000$ respectively.

where ϕ_k 's are the POD modes and a_k 's are the time-dependent coefficient called principal components. The POD spectrum and modes for chaotic components of cavity flow is shown in fig. 3.

Similar to KMD, POD is a linear expansion, but there are two major differences: the POD coordinates are uncorrelated but unlike Koopman modes, they don't necessarily evolve exponentially with time. Also the POD modes are spatially orthogonal while the Koopman modes are not necessarily so. The POD decomposition provides a robust representation of chaotic components since the modes become independent of the initial condition due to ergodicity. We will use this representation along with KMD of quasi-periodic component to approximate effect of modes on advective mixing in the flow.

3. Hypergraphs and mix-norm

In this work, we study mixing as the pure advection of passive tracers and scalar fields with the flow. In other words, we focus on the mixing process at the limit of infinitely large *Peclet* number and zero *Stokes* number. To this end, we use two different tools: We

employ *hypergraphs* to visualize mixing of each flow and do qualitative analysis. We use *mix-norm* to quantify the contribution of Koopman and POD modes to mixing of the cavity flow.

3.1. Hypergraphs

The hypergraphs are visualizations of a scalar field known as *mesohyperbolicity* which partitions the flow domain according to the type of Lagrangian deformation (Mezić *et al.* 2010). The field of mesohyperbolicity is defined as follows: Consider the trajectory of a passive tracer passing through \mathbf{x} at time t_0 . We denote by $\mathbf{u}_{t_0}^{*t_0+T}(\mathbf{x})$, the time-averaged Lagrangian velocity of the tracer over the time interval $[t_0, t_0+T]$. The mesohyperbolicity field at the location \mathbf{x} and time T is given by

$$M(\mathbf{x}, t_0, T) \equiv \det \left| \nabla_{\mathbf{x}} \mathbf{u}_{t_0}^{*t_0+T}(\mathbf{x}) \right|. \quad (3.1)$$

This field uniquely determines the type of Lagrangian fluid deformation in the neighborhood of the tracer. In particular,

1. In the regions where $M < 0$, the small patch of fluid around the tracer will be stretched in one direction and contracted in the other while moving during the next T seconds. This deformation is similar to behavior of trajectories in vicinity of a hyperbolic fixed point in a plane, hence called *mesohyperbolic*.

2. When $0 \leq M \leq 4/T^2$, the fluid patch undergoes rotation while traveling. We call this behavior *mesoelliptic*.

3. The regions with $M > 4/T^2$ show the combination of the above deformations, i.e., the fluid patch rotates while it is stretched in one direction and contracted in the other. This type of deformation is called *mesohelical*.

In the hypergraphs plotted in this paper, the mesohyperbolic behavior is marked by blue, mesoelliptic by green, and mesohelical by red. A hypergraph of the periodic cavity flow is shown in fig. 4 (right). A comparison with the Poincaré map of the same flow (left) shows how hypergraphs can be used to qualitatively assess mixing: The well-mixed regions are revealed in hypergraphs as areas with a fine-grained mixture of the mesohyperbolic and mesohelical deformation (red and blue) - similar to hyperbolic sets in dynamical systems theory. On the other hand, the islands of periodic motion which correspond to poorly mixed regions stand out as concentric bands of alternating colors.

Mezić *et al.* (2010) introduced the hypergraphs to study of finite-time (or aperiodic) mixing in 2D incompressible flows which cannot be studied via Poincaré maps. Over finite time intervals, the regions of substantial mixing stand out in hypergraphs as areas with a fine-grained combination of red and blue - similar to periodic flows, because those regions host an extensive amount of stretching and folding of the material elements, which resembles classic notion of chaotic motion. On the other hand, the poorly mixed regions divide into two subgroups: regions that are consistently meso-elliptic and therefore show rotation and stagnation zones, and regions with a dominant type of either mesohyperbolic (blue) or meso-elliptic (red) which denote likely passages for tracer motion in the form of coherent blobs. Budišić *et al.* (2016) provides a more detailed discussion of hypergraph analysis and its extension to 3D.

3.1.1. Computation and visualization of hypergraphs

Consider the trajectory of a passive tracer starting at \mathbf{x} at time t_0 . The position of this tracer at time $t > t_0$ is given by the flow map $\mathbf{F}(\mathbf{x}, t)$, which solves the ordinary differential equation (ODE)

$$\dot{\mathbf{F}}(\mathbf{x}, t) = \mathbf{u}(\mathbf{F}(\mathbf{x}, t), t), \quad t \in [t_0, t_0 + T], \quad \mathbf{F}(\mathbf{x}, t_0) = \mathbf{x}, \quad (3.2)$$

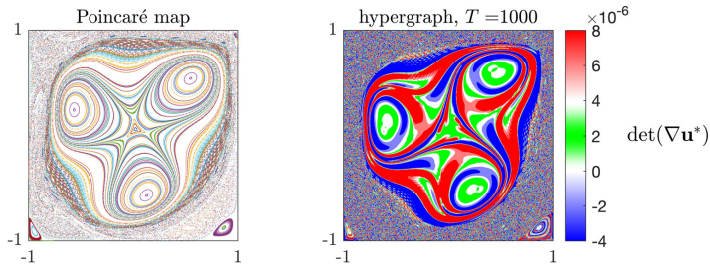


FIGURE 4. (a) Poincaré map of periodic cavity flow at $Re = 13000$, computed using 300 random trajectories over 2000 time periods. (b) Hypergraph of the same flow over 1000 sec, computed on a grid of 300×300 initial conditions. Blue, red and green colors correspond to mesohyperbolic, mesohelical and mesoelliptic behavior respectively. The (chaotic) mixing zones stand out in the hypergraph as regions with fine mixtures of red and blue.

where \mathbf{u} denotes the velocity field. The average Lagrangian velocity of the tracer is related to the flow map via

$$\mathbf{u}_{t_0}^{*t_0+T}(\mathbf{x}) = \frac{1}{T}(\mathbf{F}(\mathbf{x}, t_0 + T) - \mathbf{x}). \quad (3.3)$$

Computing the mesohyperbolicity field defined in (3.1) requires two steps of computation. First is to solve the ODE in (3.2). This is often achieved by direct integration for a grid of passive tracers initially distributed over the flow domain. The second step is to evaluate the gradient of lagrangian velocity. There are two approaches to accomplish this step. In the first approach, the gradient is computed via finite difference on the initial grid of tracers. An auxiliary grid collocated around points of the initial grid can be used to improve the numerical efficiency (see e.g. the computation of the flow map gradient by Farazmand & Haller 2012). In the second approach, which we take here, the use of finite difference is avoided by integrating the variational equation for the flow map gradient (Anosov & Arnold 1994),

$$\frac{d}{dt} \nabla \mathbf{F}(\mathbf{x}, t) = \nabla \mathbf{u}(\mathbf{F}(\mathbf{x}, t), t) \cdot \nabla \mathbf{F}(\mathbf{x}, t), \quad t \in [t_0, t_0 + T], \quad \nabla \mathbf{F}(\mathbf{x}, t_0) = I, \quad (3.4)$$

with I being the identity matrix. This ODE is solved along with (3.2) for the same set of tracers. The Lagrangian velocity gradient is given by

$$\nabla \mathbf{u}_{t_0}^{*t_0+T}(\mathbf{x}) = \frac{1}{T}(\nabla \mathbf{F}(\mathbf{x}, t_0 + T) - I). \quad (3.5)$$

This approach requires nearly the same computational effort as the finite difference approach, given that the instantaneous field of $\nabla \mathbf{u}$ is readily available. We used the standard 4th-order Runge-Kutta method to integrate equations (3.2) and (3.4). In doing so, the velocity field obtained by numerical solution of Navier-Stokes equations was interpolated using the spline method in space, and the linear method in time. In the hypergraphs plotted in this paper, the mesohyperbolicity field, $M(\mathbf{x}) := \det |\nabla \mathbf{u}_{t_0}^{*t_0+T}(\mathbf{x})|$, is plotted and partitioned into the mesohyperbolic ($M < 0$), mesoelliptic ($0 < M < 4/T^2$), and mesohelical ($M > 4/T^2$) regions, which are respectively marked by blue, green and red colors. For more readability, the value of mesohyperbolicity field in hypergraphs is cut off for $M > 8/T^2$ and $M < -4/T^2$.

3.2. *mix-norm*

We will use the evolution of a generic initial scalar field to see how well the modal approximations of the flow approximate the mixing process. Consider the scalar field $c(\mathbf{x}, t)$ which could represent concentration of dye. In absence of diffusion, c evolves in time due to the advection by the velocity field,

$$\frac{\partial c}{\partial t} + \mathbf{u} \cdot \nabla c = 0. \quad (3.6)$$

We compute the time evolution of c using a semi-Lagrangian scheme: To compute the advection of c over the time interval $[t_1, t_2]$, we put a regular grid on the flow domain at time t_2 , and advect the grid points backward in time to t_1 . Then we interpolate the field of $c(\mathbf{x}, t_1)$ onto the advected grid points. We trace back each advected point to its location on the original grid at time t_2 and assign the interpolated value to that location. The semi-Lagrangian scheme harbors much less numerical diffusion than PDE solution methods and therefore it enables a robust approximation of norms that are used for characterization of advective mixing.

There are a few measures to quantify the *mixedness* of a concentration field. In particular, the class of Sobolev-space norms with negative indices are the most popular choice for study of advection-dominated mixing. Here, we use the earliest version of such a norm introduced in [Mathew *et al.* \(2005\)](#). Let

$$c(\mathbf{x}) = \sum_{\mathbf{k} \in \mathbb{Z}^2} c_{\mathbf{k}} f_{\mathbf{k}}(\mathbf{x}) \quad (3.7)$$

be the standard Fourier expansion of c over the (bounded) flow domain. For the lid-driven cavity, \mathbf{k} is the 2-vector of wave numbers, $c_{\mathbf{k}}$'s are the Fourier coefficients, and the Fourier functions are

$$f_{\mathbf{k}}(\mathbf{x}) = e^{i2\pi(k_1x + k_2y)}. \quad (3.8)$$

Then the mix-norm of c is defined a

$$\Phi(c) = \left(\sum_{\mathbf{k} \in \mathbb{Z}^2} \frac{1}{\sqrt{1 + \pi \|\mathbf{k}\|^2}} c_{\mathbf{k}}^2 \right)^{1/2}, \quad (3.9)$$

which is similar to l^2 -norm of Fourier coefficients except that coefficients associated with higher wave numbers have smaller weights. The essential feature of this norm is that it treats mixing as a multi-scale phenomena, and puts less weight on smaller spatial scales (i.e. the weights decay as \mathbf{k} increases). When the scalar c is being mixed by the flow, its mix-norm decreases. An intuitive reasoning for this would be to note that the process of mixing stretches and folds the fluid blobs represented by large wave numbers into elongated and tightly spaced filaments represented by small wave number. We will use the above mix-norm to characterize the difference of mixing in the field $c(\mathbf{x}, t)$ according to different modal approximations of the same flow. A more detailed discussion of mix-norms is offered by [Thiffeault \(2012\)](#).

4. Slow mixing in the core and Prandtl-Batchelor theorem

Figure 5 shows the hypergraphs of mixing in cavity flow at different flow regimes and over various time intervals. The mixing in the cavity flow generally increases as the time-dependence of the velocity field is altered from periodic at $Re \approx 10500$ to fully chaotic at $Re = 30000$, but there is an outstanding feature of mixing which is common in all the flows: the mixing in the center of the cavity is slower than mixing in the areas next to

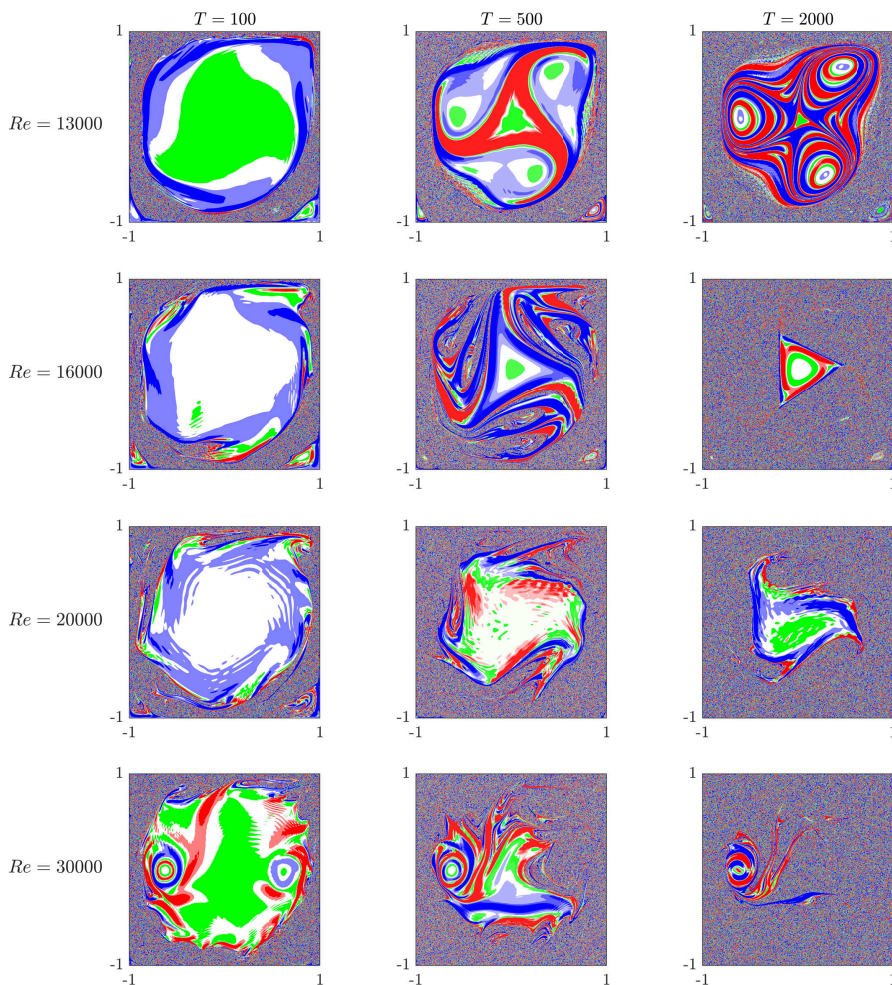


FIGURE 5. Hypergraphs of mixing in lid-driven cavity flow on interval $[0, T]$. The zones with combination of red and blue correspond to strong mixing. The figures show that mixing is slower in the center of the cavity.

the walls. For the periodic flow, the center is dominated by three periodic islands and no chaotic mixing occurs. In flows with quasi-periodicity the mixing is stronger but still it leaves a small unmixed patch in the core. In the fully chaotic flow the core gets fully mixed over long time but its mixing is substantially slower compared to the corner eddies and wall-adjacent areas. In the following, we explain this phenomenon by revisiting the Prandtl-Batchelor theorem and examining the time scales of the flow.

An important finding of all the previous studies on periodic bounded flows is that the time period of the flow is the most critical parameter that affects the mixing. The experiments by Ottino and co-workers on low-Reynolds lid-driven cavity flow, for example, have shown that the time period of the flow governs the existence and size of the

periodic islands, and therefore determines whether partial or complete mixing is achieved (Chien *et al.* 1986; Leong & Ottino 1989). Ling & Schmidt (1992) studied the influence of the flow period on the stability of periodic orbits of tracer motion and detected different ranges of flow period for which full mixing occurs. In some of those works, the relationship between flow period and the typical tracer circulation period in the steady flow was used to enhance mixing. Solomon & Mezić (2003), for instance, performed a numerical and experimental study of a 3D laminar vortex flow and observed that uniform mixing takes place when the flow period is close to the typical tracer circulation times. Another relevant example is the topological study of mixing in lid-driven cavity flow by Stremler & Chen (2007). They designed a periodic lid motion that achieves topological chaos by making a delicate match between circulation period of certain tracers and the period of the lid motion.

Here, we use the relationship between the time period of the flow and circulation period of tracers in the *mean flow* to show why mixing in the core of the cavity is poor. First note that in contrast to the aforementioned studies, the time-dependence of cavity flow in our work is due to the flow bifurcations at high Reynolds numbers. Thus the bulk of flow energy is stored in the mean flow and the unsteady component can be considered as a small perturbation to the mean flow. This is evident from the distribution of energy in the Koopman spectrum of the flow in fig. 1. Next, note that the mean flow has a critical feature which is persistent over the considered range of Reynolds number, and that feature is the relatively uniform distribution of vorticity in the central region (fig. 2). The occurrence of this so-called inviscid core in *steady* flows at high Reynolds numbers is explained by the Prandtl-Batchelor theory. The classical version of this theory states that in regions of the flow with closed streamlines and small viscous forces, the vorticity will be constant (Prandtl 1904; Batchelor 1956). In a previous work, we extended this theory to stationary time-dependent flows (Arbabi & Mezić 2019). The unsteady version of theory holds for any recirculating structure that may move with the flow, however, in the lid-driven cavity flow the location of the central vortex is almost fixed in time, and therefore averaging in time preserves the uniform distribution of vorticity in the core. Thus, we can conclude that vorticity in the core of cavity *mean flow* is uniformly distributed as well.

In the next step, we show that the uniform vorticity and closed (but not exactly circular) streamlines leads to a uniform distribution of circulation periods for Lagrangian tracers — similar to the kinematics of the rigid body rotation. We consider the nested streamlines in center of mean flow as shown on the left panel of fig. 6 and let

$$p(\psi_0) = \oint_{\psi_0} ds$$

be the perimeter of such a streamline which is the ψ_0 -level set of mean stream function. We define

$$\bar{f}(\psi_0) = \frac{\oint_{\psi_0} f(s) ds}{p(\psi_0)}, \quad (4.1)$$

to be the average of function f around that streamline. We can derive a relationship between the average of velocity magnitude on this streamline and vorticity,

$$\bar{u}(\psi_0) = \frac{\Gamma(\psi_0)}{p(\psi_0)} = \frac{\int_{A(\psi_0)} \omega dA}{p(\psi_0)} = \frac{\omega_0 A(\psi_0)}{p(\psi_0)} \quad (4.2)$$

where $\Gamma(\psi_0)$ is the circulation, and $A(\psi_0)$ is the area enclosed by the streamline. In the second equality we have used the Stokes theorem, and in the third we have used constancy

of mean vorticity from the Prandtl-Batchelor theorem. Given that the velocity on the streamline does not vanish, then the time period of circulation for a Lagrangian tracer around the streamline is given by

$$T_c(\psi_0) = \oint \frac{1}{u(s)} ds = \overline{\left(\frac{1}{u}\right)}(\psi_0) p(\psi_0). \quad (4.3)$$

Here we make the assumption that variations of velocity around the streamline is small compared to its average (e.g. the streamline is close to circular shape), that is, $u(s) = \bar{u} + u'(s)$ with $|u'(s)| \ll \bar{u}$, so that

$$\overline{\left(\frac{1}{u}\right)} = \overline{\left(\frac{1}{\bar{u} + u'}\right)} = \frac{1}{\bar{u}} \overline{\left(\frac{1}{1 + u'/\bar{u}}\right)} \approx \frac{1}{\bar{u}} \overline{(1 - u'/\bar{u})} = \frac{1}{\bar{u}}. \quad (4.4)$$

Using this approximation in (4.3), we get

$$T_c(\psi) \approx \frac{1}{\bar{u}(\psi_0)} p(\psi_0) = \frac{p^2(\psi_0)}{\omega_0 A(\psi_0)} = \frac{e(\psi_0)}{\omega_0}. \quad (4.5)$$

where we have defined $e := p^2/A$. The parameter e is a property of the shape of the streamline, and therefore two similar streamlines would have the same circulation period regardless of their size. In particular, the streamlines in the core of the mean cavity flow (fig. 6 - right panel) are quite similar which leads to almost uniform distribution of circulation period. As seen in left panel of fig. 6 the numerical computation of those time periods confirms the above analysis. In contrast, the circulation periods of the smaller vortices vary largely over shorter lengths (red, yellow and cyan curves). This observation also holds for the quasi-periodic and stationary chaotic flow.

For the special case of periodic flow, the slow mixing in the core is explained by the classical perturbation analysis of Hamiltonian systems. We consider the motion of tracers in the mean flow to be a 2D dynamical system, and the mean stream function to be its Hamiltonian. The unsteady component of the flow (i.e. sum of Koopman modes associated with nonzero frequencies) then serves as a time-periodic perturbation to the vector field of this Hamiltonian system. Then the question of the flow being well-mixed reduces to characterizing the amount of chaos present in the perturbed Hamiltonian system. There are a few techniques such as Melnikov method or Kolmogorov-Arnold-Moser (KAM) theory to predict whether any chaotic trajectories appear in such a system (Guckenheimer & Holmes 1983). The essence of these techniques is to detect the *resonances* between the circulating tracers of the mean flow and the perturbing flow field which leads to chaos, e.g., through formation of homoclinic tangles. Now if we contrast the circulation periods of the mean flow at $Re = 13000$ to the time period of the flow and its harmonics (right panel in fig. 6), we see that the motion of tracers in secondary vortices allow many resonances with the perturbing flow field, and hence, those regions contain a larger number of chaotic trajectories, whereas the flat distribution of time periods in the central vortex would not allow so many chances for resonance and therefore the amount of chaotic trajectories in the center is substantially lower. Figure 5, indeed, shows that regions of secondary corner vortices undergo substantial mixing while the core is dominated by regular trajectories.

4.1. Hypothesis testing for effect of Prandtl-Batchelor theorem on mixing

An alternative hypothesis for explanation of slow mixing in the core would be to note that the unsteady component of velocity field is weaker in the core compared to edges of the central vortex. Indeed, fig. 7(a) shows that in the first oscillatory Koopman mode

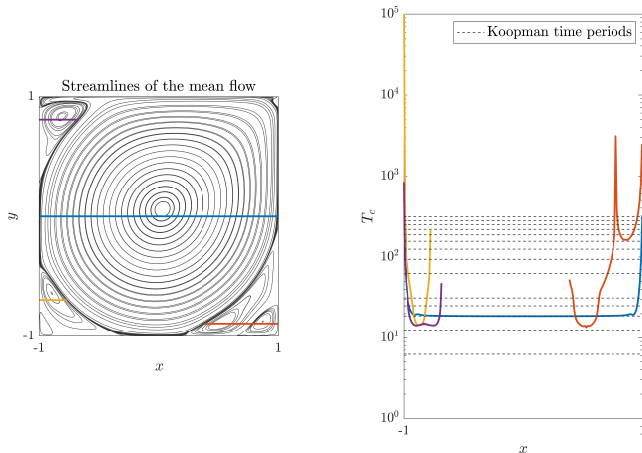


FIGURE 6. Resonance analysis for periodic mixing at $Re=13000$: Time period of tracer circulation in different zones of the mean flow (right); blue curve corresponds to a set of tracers released on the blue line in the center vortex (left) and so on. The dashed lines show some integer multiples of the (Eulerian) flow time period.

the kinetic energy is mostly distributed along the edge of the central vortex. In order to disambiguate and emphasize the effect of constant vorticity due to Prandtl-Batchelor on the mixing we conduct a numerical experiment as follows:

We first generate a random mode of velocity field $\mathbf{u}_r(x, y)$ on the cavity domain. To do so, we create a random stream function field $\psi_r(x, y) = (1 - x^4)(1 - y^4)q(x, y)$ where q is a randomly generated noise field, and then set

$$\mathbf{u}_r = \left[\frac{\partial \psi_r}{\partial y}, -\frac{\partial \psi_r}{\partial x} \right]^\top \quad (4.6)$$

We also scale \mathbf{u}_r such that its kinetic energy is equal to that of the first oscillatory Koopman mode at $Re = 13000$. This random field is, by design, zero on the boundaries, incompressible, and stronger in the core compared to the wall-adjacent areas, as shown in fig. 7(b).

We use the random field \mathbf{u}_r to perturb the velocity fields with various types of vorticity distribution and study the mixing in those perturbed flows. Consider the artificial flow model given as

$$\mathbf{u} = \mathbf{u}_b + \alpha \mathbf{u}_r e^{i\beta t}. \quad (4.7)$$

In the first model, we choose the base flow \mathbf{u}_b to be the mean of periodic flow at $Re = 13000$, and set $\alpha = 1, \beta = \omega_1$ where ω_1 is the Koopman basic frequency of the periodic flow. This model is like the actual periodic flow at $Re = 13000$, except that we have replaced the time-dependent component with a spatially random mode which oscillates at the same frequency and has the same kinetic energy. In the next two models, as the base flow we use the stable steady cavity flow at $Re = 300$ and $Re = 1000$. As shown in fig. 7(b), these two flows also have rotating cores but the tracer period distribution in their core is not as flat as the mean flow at $Re = 13000$. To put these two models on the same footing as the first model, we choose α such that the ratio $\alpha \|\mathbf{u}_r\| / \|\mathbf{u}_b\|$ is the same for all three models. Also, we choose β such that the ratio between the timescale of perturbation and the rotation time for the core is the same across the models. To be more precise, let T_c be the minimum circulation period at the core of the base flow. Then

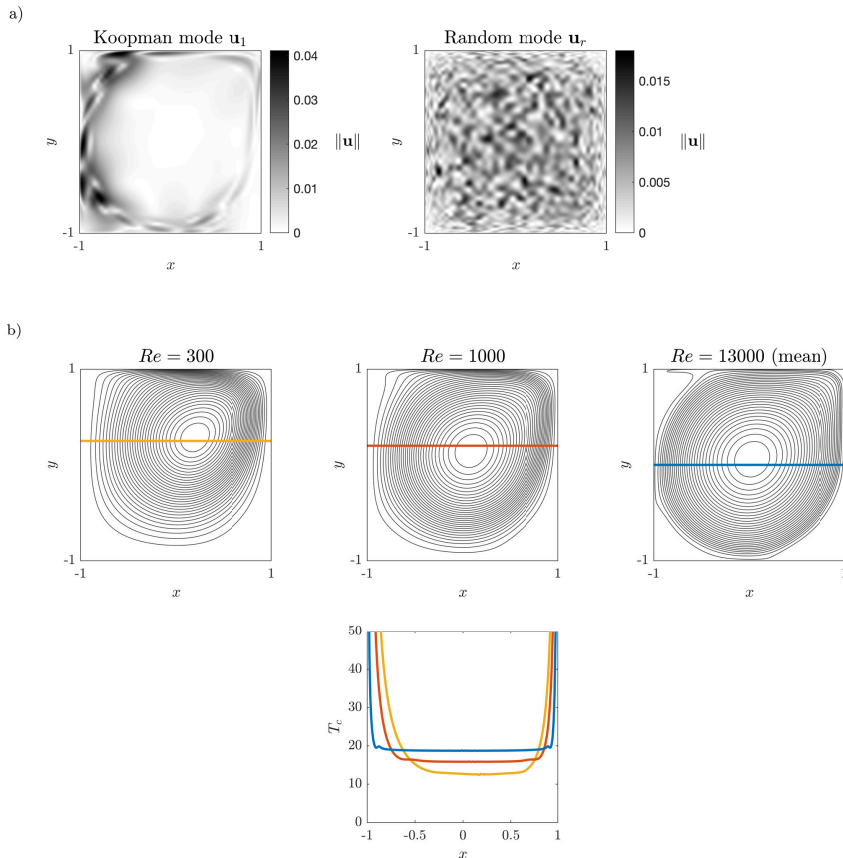


FIGURE 7. The setup for testing the effect of vorticity distribution on mixing: a) magnitude of velocity in the first oscillatory Koopman mode of $Re = 13000$ and a randomly generated velocity field with the same kinetic energy, b) top row: streamlines of central vortex in steady flows at $Re = 300, 1000$ and the mean flow at $Re = 13000$, bottom row: the tracer period distributions in those flows. We use the random field to perturb the steady flows and disambiguate the effect of vorticity distribution from the special structure of Koopman mode. T^* is (normalized) time in core rotation periods.

for all the models, we choose

$$\beta = \omega_1 \frac{T_c^{Re=13000}}{T_c}. \quad (4.8)$$

Next we compute the hypergraphs of these three models over windows of various lengths. To remove the effect of time on quality of mixing, we normalize the length of those windows by the scaling the time with respect to the core rotation time, that is, we use

$$T^* = \frac{T}{T_c}. \quad (4.9)$$

The results of the above experiment, shown in fig. 8, indicates that flatness of the circulation period makes the core of the flow more resilient to perturbations, that is, the core with a flatter distribution takes longer to mix. Therefore, it confirms the

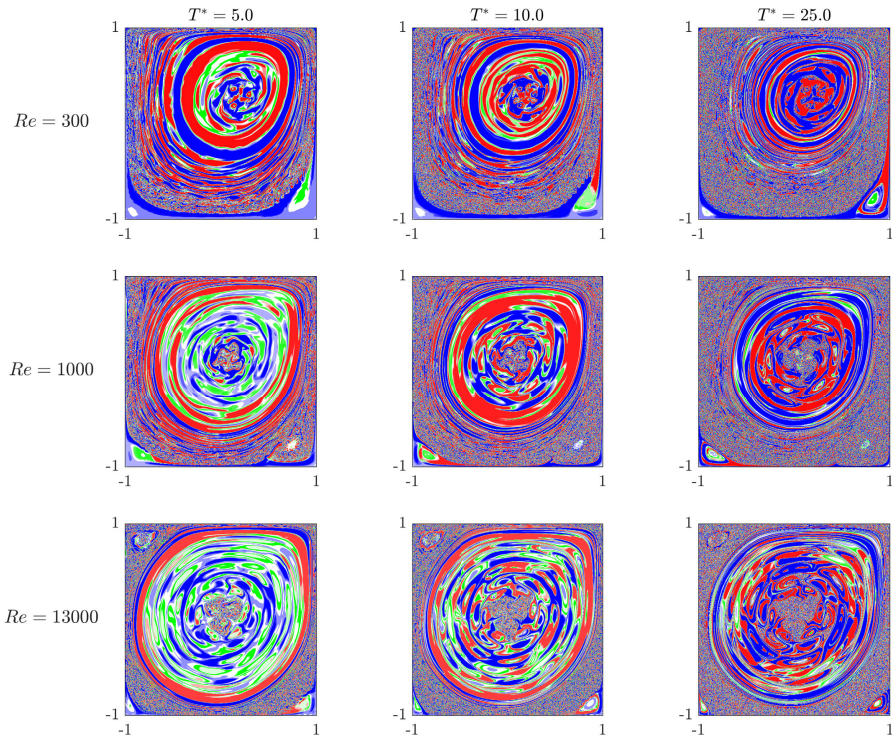


FIGURE 8. Effect of Prandtl-Batchelor theorem on mixing: hypergraphs of mean flows at various Reynolds numbers perturbed by the oscillating random field in fig. 7(a). Higher Reynolds number leads to a more uniform distribution of circulation periods in the core of mean flow and more resilience against perturbation, and hence, weaker mixing. T^* is the time window length in the core rotation units.

adverse effect of Prandtl-Batchelor theorem on mixing at high Reynolds, regardless of the spatial features of the oscillating mode. Another way to interpret this phenomenon is to note that although shear between the rotating layers of a steady flow is not enough to generate chaotic mixing, but higher shear exposed to time-dependent perturbations leads to stronger mixing. On the other hand, the Prandtl-Batchelor theorem dictates a nearly shearless core for rotational flows at high Reynolds, and hence predicts that mixing in that core is slower than other areas exposed to shear, such as areas adjacent to the walls.

Finally, we note that although the bulk of the core remains unmixed in fig. 8, a well-mixed patch emerges at their very center. This is an artifact of our experiment: The randomly generated field is much stronger than base flow at the very center and prediction of mixing with perturbation argument is not correct in that region.

4.2. Quasi-periodic and aperiodic flows

The effect of Prandtl-Batchelor theorem on mixing in quasi-periodic flow can be analyzed in a similar way. If we synthesize a new flow which consists of the mean flow and only one of basic oscillating Koopman modes, then we observe that mixing is much weaker in the core of the flow, and depending on the Koopman mode and frequency a different number of periodic islands will be formed (middle row of fig. 9). This is while the

secondary vortices undergo much faster mixing similar to the period case. Because the frequencies in a quasi-periodic flow are incommensurate, their combined harmonics (i.e. linear combination of the two basic frequencies with integer coefficients) are dense in any frequency interval. Therefore when we add the two basic oscillatory modes to the mean flow the chance of resonance with the circulation periods of the mean flow dramatically increase which leads to a larger amount of chaotic trajectories. This results in a core mixing which is stronger than the periodic flow but still weaker than the the secondary vortices and next to walls.

The above analysis cannot be readily extended to flows with chaotic time dependence. However, the evolution of stationary chaotic systems over any finite time interval can be approximated with arbitrary accuracy using quasi-periodic evolution (see e.g. [Korda et al. 2018](#)). Therefore, the finite-time mixing of the stationary chaotic flow resembles a quasi-periodic model with sufficiently many oscillatory modes. The number of modes and frequencies required to approximate the chaotic component are typically large which leads to generally faster mixing, but following the same analysis as quasi-period flows the mixing in the core will be slower than secondary vortices. This explains the picture of mixing at $Re = 30000$ in [fig. 5](#).

The resilience of rotational cores toward mixing at high Reynolds numbers has been already observed in the context of geophysical flows. [Geyer et al. \(2010\)](#) have measured mixing in an estuary where a fresh water plume from the river is flowing onto the saline water from the ocean. The measurements show that the cores of Kelvin-Helmholtz vortices formed at the interface of the fluid layers exhibit poor mixing and the bulk of mixing is occurring at the edge of those vortices and the thin filaments that connect them. They contrast their result with the previous numerical and experimental studies which are carried out at moderate and low Reynolds and conclude that the weak mixing in the core is a characteristic of high Reynolds number. In their study this behavior is attributed to the shear instabilities in the edge of vortices and connecting filaments. The analysis in the above paragraphs supports this characterization from a kinematic standpoint, namely, the Prandtl-Batchelor theory of unsteady flows predicts an almost inviscid core at high Reynolds, and the ensuing rigid-body type motion of tracers in the core makes it more resilient toward advective mixing when it is exposed to small-amplitude unsteady perturbations. We note that our arguments are based on analysis of homogenous 2D flows, and therefore their extension to 3D stratified flows requires further study.

5. Approximation of mixing using projected models

Our goal is to quantify the contribution of modes of velocity field to the mixing in the flow. This is helpful for several purposes: first, since Koopman modes are related to the state-space dynamics of the flow, identifying critical modes and associated frequencies helps in creating flow control strategies for manipulation of mixing. Second, given the theory of chaotic advection and our understanding of mixing in periodic flows, and to a lesser degree quasi-periodic flows, we are interested in understanding how well low-complexity approximations of the flow can approximate the mixing in the actual flow. Indeed, in the previous section we used models of the flow involving mean flow and oscillatory modes to study mixing. We use Koopman modes and POD modes in our analysis, mainly because the Koopman and POD modes are the most economical choices for constructing low-dimensional approximations of, respectively, the quasi-periodic and chaotic components of the flow ([Holmes et al. 2012](#); [Arbabi & Mezić 2017](#)). Moreover, there are a number of data reconstruction methods ([Bui-Thanh et al. 2004](#)) and many

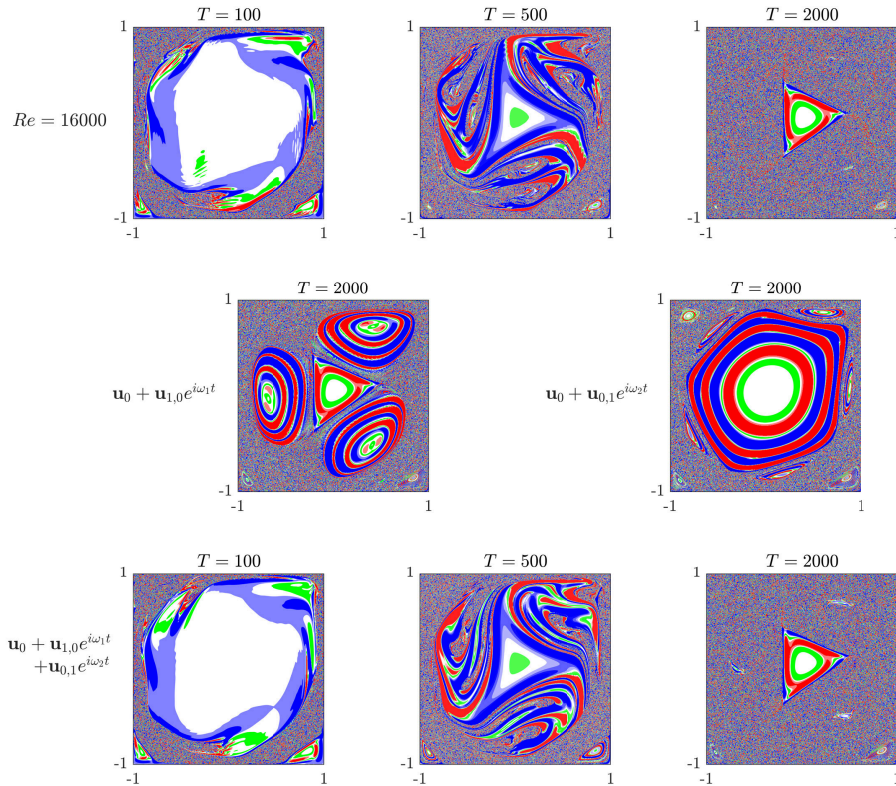


FIGURE 9. Hypergraphs of the quasi-periodic flow repeated from fig. 5 (top), hypergraphs of flow models each consisting of the mean flow and one basic Koopman mode (middle), and hypergraphs of a flow model consisting of the mean flow and both basic Koopman modes (bottom). The resonances between the two oscillatory modes leads to stronger mixing in the core compared to periodic flow but still slower compared to wall-adjacent areas.

model reduction techniques (Cazemier *et al.* 1998; Noack *et al.* 2003) that rely on modal decompositions such as POD. Our analysis informs us about the suitable dimension of modal decomposition or appropriate level of “denoising” in those methods for an accurate reproduction of mixing behavior.

We first construct projected models of the flow which contain only subset of Koopman and POD modes. Given the definition and notation of KMD and POD in section 2, we define a projected model as

$$\mathbf{u}_{n_k, n_p}(\mathbf{x}, t) = \sum_{j=1}^{n_k} \mathbf{u}_j(\mathbf{x}) e^{i\omega_j t} + \sum_{l=1}^{n_p} \phi_l(\mathbf{x}) a_l(t), \quad (5.1)$$

where n_k and n_p denote the number of Koopman and POD modes used in the model. In forming the above expansion, we stack the modes by starting from the Koopman modes in the order of decreasing energy and then use the POD modes of the chaotic component with the same ordering.

We compare the mixing in the flow and its projected model using the following

numerical experiment: we define an initial blob of concentration as shown on top of fig. 10. Then we advect this blob in the actual flow as well as the projected models. Then over regular intervals we measure how much the advected concentration field in the projected flows is deviated from the actual flow by defining

$$e(t) = \frac{\Phi(\Delta c(\mathbf{x}, t))}{\Phi(c(\mathbf{x}, 0))} \quad (5.2)$$

where $c(\Delta \mathbf{x}, t)$ is the difference of the concentration fields, $c(\mathbf{x}, t)$ is the initial concentration field corresponding to the rectangular blob and $\Phi(\cdot)$ is the mix-norm defined in (3.9). Note that the results of this experiment depends on the initial condition of the blob, however, through several trials, we have chosen the initial position so that the experiment to incorporate mixing near and away from the walls (fig. 10) and give a clear and general picture of mixing.

Figure 11 shows the results of the experiment over an interval of length 200 which is about 10 times the circulation period in the core of mean flow. At the start the deviation rapidly grows from zero due to difference in velocity fields (this growth is not shown in the log-log plot) but as the time passes the rate of error growth slows down because the mixing process transfers more concentration to small scales which reduces the mix-norm. The mixing error shows that the periodic flow has the lowest complexity in the sense that two Koopman modes (i.e. mean flow + basic oscillatory mode) are enough to describe the advection of the blob within an accuracy of a few percents over long times. In the quasi-periodic flow, the energy of unsteady part is distributed among a larger number of modes, as such the number of modes required to achieve %1 accuracy is close to the total number of Koopman modes.

The number of modes required for accurate prediction of mixing drastically increases when continuous spectrum is present. As fig. 11 suggests, to achieve %1 accuracy in estimation of a blob advection we need at least a few hundred POD modes in addition to Koopman modes in our model. Conversely, the projected models that contain %99 of the flow energy approximate mixing with %2–4 error after one circulation period. This error rises, rather gently, to about %10 percent after about 10 circulation period. Although difference in the velocity fields leads to exponential divergence of tracer trajectories, the result of this experiment shows that accuracy of global mixing over short times (i.e. a few advective time scales) is proportional to accuracy of the Eulerian field in the projected model. This implies that flow dynamics reconstructed by data assimilation or model reduction methods can provide accurate resolutions of mixing in the target flow given a sufficiently high-dimensional reconstruction of the Eulerian flow field.

6. Summary

An interesting feature of 2D cavity flow at high Reynolds numbers is that mixing in its core is weaker compared to the corner eddies. In this paper, we explained this observation through a combination of ideas from fluid mechanics and dynamical systems. Namely, we showed that the circulation periods in the mean flow have a flat distribution in the core as a consequence of Prandtl-Batchelor theorem, and the poor mixing is the result of the interaction between this flat distribution and the time scales of Eulerian flow perturbations — unsteady components of the flow which possess small amplitudes compared to the mean flow. This analysis supports the field observations that show poor mixing in the core of Kelvin-Helmholtz vortices at high Reynolds.

We also characterized the contribution fo Koopman and POD modes to mixing at various Reynolds numbers by comparing the advection of generic blob in the actual

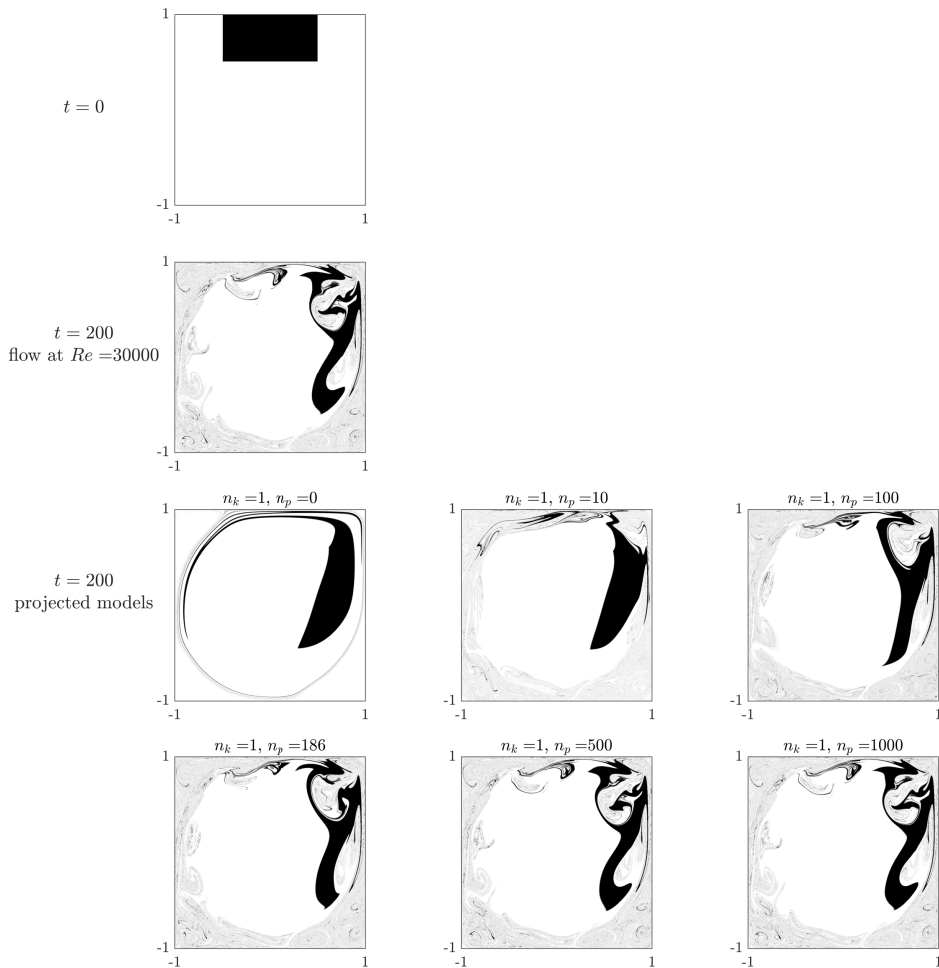


FIGURE 10. The initial concentration field (first row), concentration field advected by the flow (second row), and concentration field advected by the projected models defined in (5.1) (bottom rows). n_k and n_p are, respectively, the number of Koopman and POD modes in the projected model.

flow versus projected models of flow consisting of a subset of those modes. Our analysis showed that mixing of periodic and quasi-periodic flows can be accurately described by a handful of Koopman modes, and while for flows with continuous spectrum the number of required modes grow much larger, projected models made of sufficiently large number of POD modes (e.g. resolving %99 of kinetic energy) provide an accurate estimation of mixing over a few advective time scales.

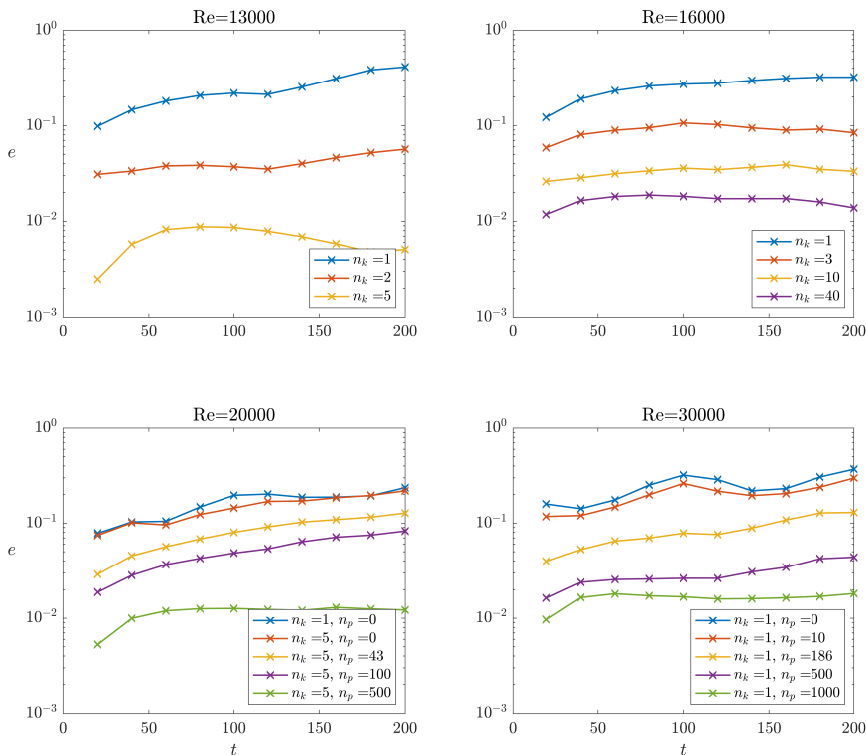


FIGURE 11. Mix-norm error of mixing approximation using projected models. n_k and n_p denote the number of Koopman modes and POD modes in a projected model. The projected model with $n_p = 43$ and $n_p = 186$ resolve %99 of the unsteady kinetic energy in the flow at $Re = 20000$ and $Re = 30000$ respectively.

7. Acknowledgement and source code

This research was partially supported by the ONR grant N00014-14-1-0633. H. A. thanks Pierre-Yves Passaggia for an informative discussion and introducing references on mixing in stratified flows and S. Mohammad Mirzadeh for helpful notes on advection simulations. We are also grateful to L. Gary Leal for comments and questions that improved this manuscript.

The MATLAB implementation of advection, mix-norm and hypergraphs computation along with the flow data used in the paper is available at <https://github.com/arbabiha/Mixing-analysis-2d-flows>.

REFERENCES

- ANDERSON, PD, GALAKTIONOV, OS, PETERS, GWM, VAN DE VOSSE, FN & MEIJER, HEH 1999 Analysis of mixing in three-dimensional time-periodic cavity flows. *Journal of Fluid Mechanics* **386**, 149–166.
- ANDERSON, PATRICK D, GALAKTIONOV, OLEKSIY S, PETERS, GERRIT WM, VAN DE VOSSE, FRANS N & MEIJER, HAN EH 2000 Chaotic fluid mixing in non-quasi-static time-periodic cavity flows. *International journal of heat and fluid flow* **21** (2), 176–185.

- ANOSOV, DV & ARNOLD, VI 1994 *Dynamical System I, Ordinary Differential Equations and Smooth Dynamical Systems*. Springer Verlag.
- ARBABI, HASSAN & MEZIĆ, IGOR 2017 Study of dynamics in post-transient flows using Koopman mode decomposition. *Phys. Rev. Fluids* **2**, 124402.
- ARBABI, HASSAN & MEZIĆ, IGOR 2019 Prandtl–batchelor theorem for flows with quasiperiodic time dependence. *Journal of Fluid Mechanics* **862**.
- AREF, HASSAN 1984 Stirring by chaotic advection. *Journal of fluid mechanics* **143**, 1–21.
- BATCHELOR, G K 1956 On steady laminar flow with closed streamlines at large reynolds number. *Journal of Fluid Mechanics* **1** (02), 177–190.
- BOYLAND, PHILIP L, AREF, HASSAN & STREMLER, MARK A 2000 Topological fluid mechanics of stirring. *Journal of Fluid Mechanics* **403**, 277–304.
- BUDIŠIĆ, MARKO & THIFFEAULT, JEAN-LUC 2015 Finite-time braiding exponents. *Chaos: An Interdisciplinary Journal of Nonlinear Science* **25** (8), 087407.
- BUDIŠIĆ, MARKO, SIEGMUND, STEFAN, SON, DOAN THAI & MEZIĆ, IGOR 2016 Mesochronic classification of trajectories in incompressible 3D vector fields over finite times. *Discrete and Continuous Dynamical Systems - Series S* **9** (4), 923–958.
- BUI-THANH, TAN, DAMODARAN, MURALI & WILLCOX, KAREN E 2004 Aerodynamic data reconstruction and inverse design using proper orthogonal decomposition. *AIAA journal* **42** (8), 1505–1516.
- CAZEMIER, W, VERSTAPPEN, RWCP & VELDMAN, AEP 1998 Proper orthogonal decomposition and low-dimensional models for driven cavity flows. *Physics of Fluids (1994-present)* **10** (7), 1685–1699.
- CHAKRAVARTHY, VS & OTTINO, JM 1996 Mixing of two viscous fluids in a rectangular cavity. *Chemical engineering science* **51** (14), 3613–3622.
- CHELLA, RAVINDRAN & OTTINO, JULIO M 1985 Fluid mechanics of mixing in a single-screw extruder. *Industrial & engineering chemistry fundamentals* **24** (2), 170–180.
- CHELLA, RAVI & VIÑALS, JORGE 1996 Mixing of a two-phase fluid by cavity flow. *Physical Review E* **53** (4), 3832.
- CHIEN, WL, RISING, H & OTTINO, JM 1986 Laminar mixing and chaotic mixing in several cavity flows. *Journal of Fluid Mechanics* **170** (1), 355–377.
- COULLETTE, CHAD, LEKIEN, FRANCOIS, PADUAN, JEFFREY D, HALLER, GEORGE & MARSDEN, JERROLD E 2007 Optimal pollution mitigation in monterey bay based on coastal radar data and nonlinear dynamics. *Environmental science & technology* **41** (18), 6562–6572.
- FARAZMAND, MOHAMMAD & HALLER, GEORGE 2012 Computing Lagrangian coherent structures from their variational theory. *Chaos (Woodbury, N.Y.)* **22** (1), 013128.
- FERRACHAT, SYLVAIN & RICARD, YANICK 2001 Mixing properties in the earth’s mantle: effects of the viscosity stratification and of oceanic crust segregation. *Geochemistry, Geophysics, Geosystems* **2** (4).
- FRANJIONE, JOHN G, LEONG, CHIK-WENG & OTTINO, JULIO M 1989 Symmetries within chaos: a route to effective mixing. *Physics of Fluids A: Fluid Dynamics (1989-1993)* **1** (11), 1772–1783.
- FROYLAND, GARY, SANTITISSADEEKORN, NARATIP & MONAHAN, ADAM 2010 Transport in time-dependent dynamical systems: Finite-time coherent sets. *Chaos: An Interdisciplinary Journal of Nonlinear Science* **20** (4), 043116.
- GEYER, W ROCKWELL, LAVERY, ANDONE C, SCULLY, MALCOLM E & TROWBRIDGE, JOHN H 2010 Mixing by shear instability at high reynolds number. *Geophysical Research Letters* **37** (22).
- GHARIB, MORTEZA & DERANGO, PHILIP 1989 A liquid film (soap film) tunnel to study two-dimensional laminar and turbulent shear flows. *Physica D: Nonlinear Phenomena* **37** (1-3), 406–416.
- GHIA, UKNG, GHIA, KIRTI N & SHIN, CT 1982 High-re solutions for incompressible flow using the navier-stokes equations and a multigrid method. *Journal of computational physics* **48** (3), 387–411.
- GUCKENHEIMER, JOHN & HOLMES, PHILIP 1983 Nonlinear oscillations, dynamical systems, and bifurcations of vector fields .
- HALLER, G. 2015 Lagrangian Coherent Structures. *Annual Review of Fluid Mechanics* **47** (1).

- HOLMES, PHILIP, LUMLEY, JOHN L, BERKOOZ, GAL & ROWLEY, CLARENCE 2012 *Turbulence, coherent structures, dynamical systems and symmetry*. Cambridge university press.
- HWANG, WOOK RYOL, ANDERSON, PATRICK D & HULSEN, MARTIEN A 2005 Chaotic advection in a cavity flow with rigid particles. *Physics of fluids* **17** (4), 043602.
- JANA, SADHAN C, METCALFE, GUY & OTTINO, JM 1994a Experimental and computational studies of mixing in complex stokes flows: the vortex mixing flow and multicellular cavity flows. *Journal of Fluid Mechanics* **269**, 199–246.
- JANA, SADHAN C, TJAHHADI, MAHARI & OTTINO, JM 1994b Chaotic mixing of viscous fluids by periodic changes in geometry: baffled cavity flow. *AIChE journal* **40** (11), 1769–1781.
- KHAKHAR, DV, FRANJIONE, JG & OTTINO, JM 1987 A case study of chaotic mixing in deterministic flows: the partitioned-pipe mixer. *Chemical Engineering Science* **42** (12), 2909–2926.
- KOOPMAN, BERNARD O 1931 Hamiltonian systems and transformation in hilbert space. *Proceedings of the National Academy of Sciences* **17** (5), 315–318.
- KORDA, MILAN, PUTINAR, MIHAI & MEZIĆ, IGOR 2018 Data-driven spectral analysis of the koopman operator. *Applied and Computational Harmonic Analysis* .
- KOSEFF, JR & STREET, RL 1984 The lid-driven cavity flow: a synthesis of qualitative and quantitative observations. *Journal of Fluids Engineering* **106** (4), 390–398.
- LARGE, WILLIAM G, MCWILLIAMS, JAMES C & DONEY, SCOTT C 1994 Oceanic vertical mixing: A review and a model with a nonlocal boundary layer parameterization. *Reviews of Geophysics* **32** (4), 363–403.
- LEONG, CW & OTTINO, JM 1989 Experiments on mixing due to chaotic advection in a cavity. *Journal of Fluid Mechanics* **209**, 463–499.
- LING, FH 1993 The effect of mixing protocol on mixing in discontinuous cavity flows. *Physics Letters A* **177** (4-5), 331–337.
- LING, FH & SCHMIDT, G 1992 Mixing windows in discontinuous cavity flows. *Physics Letters A* **165** (3), 221–230.
- LIU, M, MUZZIO, FJ & PESKIN, RL 1994 Quantification of mixing in aperiodic chaotic flows. *Chaos, Solitons & Fractals* **4** (6), 869–893.
- MATHEW, GEORGE, MEZIĆ, IGOR & PETZOLD, LINDA 2005 A multiscale measure for mixing. *Physica D: Nonlinear Phenomena* **211** (1), 23–46.
- MELESHKO, VV & PETERS, GWM 1996 Periodic points for two-dimensional stokes flow in a rectangular cavity. *Physics Letters A* **216** (1), 87–96.
- MEZIĆ, IGOR 2005 Spectral properties of dynamical systems, model reduction and decompositions. *Nonlinear Dynamics* **41** (1-3), 309–325.
- MEZIĆ, IGOR 2013 Analysis of fluid flows via spectral properties of the Koopman operator. *Annual Review of Fluid Mechanics* **45**, 357–378.
- MEZIĆ, IGOR & BANASZUK, ANDRZEJ 2004 Comparison of systems with complex behavior. *Physica D: Nonlinear Phenomena* **197** (1), 101–133.
- MEZIĆ, IGOR, LOIRE, S, FONBEROV, VLADIMIR A & HOGAN, P 2010 A new mixing diagnostic and gulf oil spill movement. *Science* **330** (6003), 486–489.
- MIGEON, C, TEXIER, A & PINEAU, G 2000 Effects of lid-driven cavity shape on the flow establishment phase. *Journal of Fluids and Structures* **14** (4), 469–488.
- NOACK, BERND R, AFANASIEV, KONSTANTIN, MORZYNSKI, MAREK, TADMOR, GILEAD & THIELE, FRANK 2003 A hierarchy of low-dimensional models for the transient and post-transient cylinder wake. *Journal of Fluid Mechanics* **497**, 335–363.
- OTTINO, JM, MUZZIO, FJ, TJAHHADI, M, FRANJIONE, JG, JANA, SC & KUSCH, HA 1992 Chaos, symmetry, and self-similarity- exploiting order and disorder in mixing processes. *Science* **257** (5071), 754–760.
- OTTINO, JULIO M 1989 *The kinematics of mixing: stretching, chaos, and transport*, , vol. 3. Cambridge university press.
- PAI, SA, PRAKASH, P & PATNAIK, BSV 2013 Numerical simulation of chaotic mixing in lid driven cavity: effect of passive plug. *Engineering Applications of Computational Fluid Mechanics* **7** (3), 406–418.
- POJE, ANDREW C, HALLER, GEORGE & MEZIĆ, I 1999 The geometry and statistics of mixing in aperiodic flows. *Physics of Fluids (1994-present)* **11** (10), 2963–2968.

- PRANDTL, LUDWIG 1904 Über flüssigkeits bewegung bei sehr kleiner reibung. *Verhaldlg III Int. Math. Kong* pp. 484–491.
- ROM-KEDAR, V, LEONARD, A & WIGGINS, S 1990 An analytical study of transport, mixing and chaos in an unsteady vortical flow. *Journal of Fluid Mechanics* **214**, 347–394.
- ROWLEY, C.W., MEZIĆ, I., BAGHERI, S., SCHLATTER, P. & HENNINGSON, D.S. 2009 Spectral analysis of nonlinear flows. *Journal of Fluid Mechanics* **641** (1), 115–127.
- SCHMID, PETER J 2010 Dynamic mode decomposition of numerical and experimental data. *Journal of Fluid Mechanics* **656**, 5–28.
- SHADDEN, SHAWN C & TAYLOR, CHARLES A 2008 Characterization of coherent structures in the cardiovascular system. *Annals of biomedical engineering* **36** (7), 1152–1162.
- SHERWOOD, STEVEN C, BONY, SANDRINE & DUFRESNE, JEAN-LOUIS 2014 Spread in model climate sensitivity traced to atmospheric convective mixing. *Nature* **505** (7481), 37–42.
- SOLOMON, TH & MEZIĆ, IGOR 2003 Uniform resonant chaotic mixing in fluid flows. *Nature* **425** (6956), 376–380.
- STREMLER, MARK A & CHEN, JIE 2007 Generating topological chaos in lid-driven cavity flow. *Physics of Fluids (1994-present)* **19** (10), 103602.
- STROOCK, ABRAHAM D, DERTINGER, STEPHAN KW, AJDARI, ARMAND, MEZIĆ, IGOR, STONE, HOWARD A & WHITESIDES, GEORGE M 2002 Chaotic mixer for microchannels. *Science* **295** (5555), 647–651.
- THIFFEAULT, JEAN-LUC 2012 Using multiscale norms to quantify mixing and transport. *Nonlinearity* **25** (2), R1.
- TSENG, YU-HENG & FERZIGER, JOEL H 2001 Mixing and available potential energy in stratified flows. *Physics of Fluids* **13** (5), 1281–1293.
- VALENTINE, DAVID L, MEZIĆ, IGOR, MAČEŠIĆ, SENKA, ČRNJARIĆ-ŽIĆ, NELIDA, IVIĆ, STEFAN, HOGAN, PATRICK J, FONOBEROV, VLADIMIR A & LOIRE, SOPHIE 2012 Dynamic autoinoculation and the microbial ecology of a deep water hydrocarbon irruption. *Proceedings of the National Academy of Sciences* **109** (50), 20286–20291.
- VIKHANSKY, A 2003 Chaotic advection of finite-size bodies in a cavity flow. *physics of fluids* **15** (7), 1830–1836.